Soft Matter

RSC Publishing

PAPER

View Article Online
View Journal | View Issue

Bubble nucleation in polymer–CO_2 mixtures

Cite this: *Soft Matter*, 2013, **9**, 9675

Xiaofei Xu,[a] Diego E. Cristancho,[b] Stéphane Costeux[b] and Zhen-Gang Wang*[a]

Received 26th May 2013
Accepted 3rd August 2013

DOI: 10.1039/c3sm51477c

www.rsc.org/softmatter

We combine density-functional theory with the string method to calculate the minimum free energy path of bubble nucleation in two polymer–CO_2 mixture systems, poly(methyl methacrylate) (PMMA)–CO_2 and polystyrene (PS)–CO_2. Nucleation is initiated by saturating the polymer liquid with high pressure CO_2 and subsequently reducing the pressure to ambient condition. Below a critical temperature (T_c), we find that there is a discontinuous drop in the nucleation barrier as a function of increased initial CO_2 pressure (P_0), as a result of an underlying metastable transition from a CO_2-rich-vapor phase to a CO_2-rich-liquid phase. The nucleation barrier is generally higher for PS–CO_2 than for PMMA–CO_2 under the same temperature and pressure conditions, and both higher temperature and higher initial pressure are required to lower the nucleation barrier for PS–CO_2 to experimentally relevant ranges. Classical nucleation theory completely fails to capture the structural features of the bubble nucleus and severely underestimates the nucleation barrier.

1. Introduction

Bubble nucleation in polymer–carbon dioxide (CO_2) mixtures is a problem of great interest in the manufacturing of polymer foams since it plays a crucial role in determining the cell size and pore density of the foam materials.[1] As a fundamental problem, bubble nucleation in polymer–CO_2 is a rich and complex problem because of the finite compressibility of the mixture and possible interplay between liquid–vapor transition and liquid–liquid phase separation.[2–5] For example, Müller *et al.*[6] showed that the nucleation behavior and the structure of the critical nucleus are strongly affected by the proximity to the (polymer-rich liquid, CO_2-rich vapor and CO_2-rich liquid) triple point.

A quantitative theory that predicts the bubble nucleation behavior in polymer–CO_2 mixtures as a function of the pressure, temperature and composition can be a valuable tool for rationally controlling the foaming conditions and can also contribute to the fundamental understanding of nucleation in compressible binary mixtures in general.[3,5,6] However, such a theory has not been available owing to the lack of accurate description of the thermodynamic and interfacial properties of the polymer–CO_2 mixtures at the molecular level.[2,3] Direct molecular simulation of the nucleation behavior is currently impossible due to the molecular complexity of the system and the activated nature of the phenomenon. On the other hand, the classical nucleation theory (CNT) is not only unsatisfactory at the quantitative level, but can even fail to capture some qualitative features, as will be demonstrated in this work. Density-functional theory (DFT) is an attractive alternative as it can successfully capture the necessary microscopic details of nucleation.[7] DFT treats the nuclei as inhomogeneous density profiles, and the free energy of the system is given as a functional of the profiles. Effects of interfacial curvature and compressibility are incorporated automatically in the DFT description. Under a given nucleation condition, the functional has a saddle point corresponding to the critical nucleus. Nucleation is considered to proceed along the minimum free energy path (MFEP) that connects the metastable uniform bulk state to a well-developed bubble by passing through the critical nucleus.

In this work, we use our recently developed DFT[8] based on the perturbed chain-statistical associating field theory equation of state (PC-SAFT EOS)[9] to study bubble nucleation in polymer–CO_2 mixtures, using poly(methyl methacrylate) (PMMA) and polystyrene (PS) as examples for the polymer. The DFT we use for the polymer–CO_2 is built on a coarse-grained molecular model in which the CO_2 molecule is modeled as a sphere and the polymer is modeled as a freely jointed chain of tangentially connected spheres. The excluded volume of the species is represented by hard-core interactions. Energetic interactions are described by the attractive part of the Lennard-Jones potential. In addition, a weak association interaction is included between the CO_2 molecules. The DFT gives a quantitatively satisfactory description of the thermodynamic bulk and interfacial properties of polymer–CO_2 mixtures in a wide temperature and pressure range.

The evolution of the bubble along the MFEP is obtained by the string method, which is a modified steepest descent algorithm.[10] The free energy barrier and the structure of the critical nucleus are calculated by systematically examining the effect of temperature, pressure and the CO_2 content. The temperature

[a]*Division of Chemistry and Chemical Engineering, California Institute of Technology, Pasadena, CA 91125, USA. E-mail: zgw@caltech.edu*
[b]*The Dow Chemical Company, Midland, MI 48674, USA*

and pressure conditions are selected in the experimentally relevant range, *i.e.*, temperatures near the critical temperature of CO_2, and pressures in the range from ambient pressure to 10 s of mega pascal (MPa).

In a recent communication,[11] we briefly presented our result on a discontinuous nucleation behavior in the PMMA–CO_2 mixture that arises from an underlying metastable condensation transition of the CO_2-rich phase. In this work, we will explore this behavior in further detail by comparing the difference between the PS–CO_2 and PMMA–CO_2 systems. We find that the nucleation barrier is generally higher for PS–CO_2 than for PMMA–CO_2 under the same temperature and pressure conditions, which, however, is not simply due to the lower solubility of CO_2 in PS. We also evaluate the validity of CNT by comparing our results with predictions of CNT using both the equilibrium interfacial tension and an effective interfacial tension fitted from a well-developed bubble. In both cases, we find that CNT considerably underestimates the nucleation barrier.

2. Molecular model

The molecular units of both components in a compressible polymer–CO_2 mixture are coarse-grained as spherical particles with a hard core. The CO_2 molecule is modeled as a sphere. A weak association interaction is assumed between CO_2 molecules. The association interaction between the attractive sites of carbon and oxygen atoms leads to the formation of dimers, trimers, tetramers, *etc.* We account for the strength of association interaction by the average size (N_1) of the clusters. In principle, N_1 should depend on the density of CO_2 and temperature. However, for simplicity in this work we ignore such dependences, and assume N_1 to be a constant. The best numerical fitting of experimental PVT data of pure CO_2 yields $N_1 = 2$. Note also that $N_1 = 2$ is only used in the excess part of the free energy. The polymer is modeled as a freely jointed chain of tangentially connected spheres. The chain connectivity is enforced by the bonding constraint between nearest-neighbor segments,

$$\exp\left[-\beta V_B\left(\boldsymbol{r}^{N_2}\right)\right] = \prod_{i=1}^{N_2-1} \frac{\delta(|\boldsymbol{r}_{i+1} - \boldsymbol{r}_i| - \sigma_2)}{4\pi\sigma_2{}^2} \tag{1}$$

where δ is the Dirac delta function and $\boldsymbol{r}^{N_2} = (\boldsymbol{r}_1, \boldsymbol{r}_2, \ldots, \boldsymbol{r}_{N_2})$ and $\beta^{-1} = kT$ stands for the temperature multiplied by the Boltzmann constant. The interaction between two arbitrary species (*i.e.* polymer segments or CO_2) is described by

$$u_{ij}(r) = \begin{cases} \infty & r < \sigma_{ij} \\ -\varepsilon_{ij}\left(\sigma_{ij}/r\right)^6 & r \geq \sigma_{ij} \end{cases} \tag{2}$$

where $i, j = 1, 2$, with 1 denoting CO_2 and 2 denoting a polymer segment. The cross interaction is given by $\sigma_{ij} = (\sigma_i + \sigma_j)/2, \varepsilon_{ij} = \sqrt{\varepsilon_i\varepsilon_j}\,(1 - k_{ij}), (i \neq j)$. Details for the value of molecular weight (M), chain length of polymer or average size of the CO_2 cluster due to association interaction (N), energy parameter (ε), monomer diameter (σ) and k_{ij} parameter for the species used in the model are given in our recent publication.[8]

3. Density functional theory

The DFT is constructed from the PC-SAFT EOS.[9] The Helmholtz free energy functional is expressed as a sum of an ideal-gas term and excess terms accounting for the inter- and intramolecular interactions,

$$F = F^{\mathrm{id}}[\rho_1(\boldsymbol{r}), \hat{\rho}_2(\boldsymbol{r}^{N_2})] + F^{\mathrm{ex}}[\rho_1(\boldsymbol{r}), \hat{\rho}_2(\boldsymbol{r}^{N_2})] \tag{3}$$

where $\rho_1(\boldsymbol{r})$ is the density profile of CO_2. $\hat{\rho}_2(\boldsymbol{r}^{N_2})$ is the multidimensional density profile of polymer chain, *i.e.*, the joint density of all the N_2 segments of the polymer, which is related to the segmental densities ρ_{2i} ($i = 1, 2, \ldots, N_2$) by

$$\rho_2(\boldsymbol{r}) = \sum_{i=1}^{N_2} \rho_{2,i}(\boldsymbol{r}) = \sum_{i=1}^{N_2} \int \mathrm{d}\boldsymbol{r}^{N_2}\, \delta(\boldsymbol{r} - \boldsymbol{r}_i)\hat{\rho}_2\left(\boldsymbol{r}^{N_2}\right) \tag{4}$$

The ideal term of Helmholtz free energy is known exactly as

$$\begin{aligned} \beta F^{\mathrm{id}}[\rho_1(\boldsymbol{r}), \hat{\rho}_2(\boldsymbol{r}^{N_2})] = {} & \int \mathrm{d}\boldsymbol{r}\rho_1(\boldsymbol{r})[\ln\rho_1(\boldsymbol{r}) - 1] \\ & + \int \mathrm{d}\boldsymbol{r}^{N_2}\hat{\rho}_2(\boldsymbol{r}^{N_2})[\ln\hat{\rho}_2(\boldsymbol{r}^{N_2}) - 1] \\ & + \int \mathrm{d}\boldsymbol{r}^{N_2}\hat{\rho}_2(\boldsymbol{r}^{N_2})\beta V_B(\boldsymbol{r}^{N_2}) \end{aligned} \tag{5}$$

In PC-SAFT-based DFT, the excess Helmholtz free energy includes the contribution from the excluded-volume effect, correlations due to CO_2 association and polymer chain connectivity, and dispersion interactions,

$$F^{\mathrm{ex}} = F^{\mathrm{ex}}_{\mathrm{hs}} + F^{\mathrm{ex}}_{\mathrm{assoc}} + F^{\mathrm{ex}}_{\mathrm{disp\text{-}local}} + F^{\mathrm{ex}}_{\mathrm{disp\text{-}nonlocal}} \tag{6}$$

The first three terms extend the corresponding bulk terms of the PC-SAFT EOS to spatially varying systems, whereas the last term is an additional contribution due to the long-range dispersion interaction that is only non-vanishing when the system is inhomogeneous. $F^{\mathrm{ex}}_{\mathrm{hs}}$ accounts for the excluded volume effect and is given by the modified fundamental measure theory[12,13]

$$\beta F^{\mathrm{ex}}_{\mathrm{hs}} = \int \mathrm{d}\boldsymbol{r}\phi_{\mathrm{hs}}[n_\alpha(\boldsymbol{r})] \tag{7}$$

with

$$\begin{aligned} \phi_{\mathrm{hs}}[n_\alpha(\boldsymbol{r})] = {} & -n_0\ln(1 - n_3) + \frac{n_1 n_2 - \boldsymbol{n}_{V1}\boldsymbol{n}_{V2}}{1 - n_3} \\ & + \left[\frac{\ln(1 - n_3)}{12\pi n_3{}^2} + \frac{1}{12\pi n_3(1 - n_3)^2}\right]\left(n_3{}^2/3 - n_2\boldsymbol{n}_{V2}\boldsymbol{n}_{V2}\right) \end{aligned} \tag{8}$$

where $n_i[\{\rho_j(\boldsymbol{r})|j = 1, 2\}]$, ($i = 0, 1, 2, 3, V1, V2$) are the weight density functionals of Rosenfeld.[12] These weight density functionals are also used to describe other short-range interactions such as association and the local part of the dispersion interactions. We adopt the weighted density approximation (WDA) to extend these terms to inhomogeneous states. $\beta F^{\mathrm{ex}}_{\mathrm{assoc}}$ due to the polymer chain connectivity and CO_2 associating interaction is given by[14]

$$\beta F^{\mathrm{ex}}_{\mathrm{assoc}} = \sum_{i=1}^{2} \frac{1 - N_i}{N_i} \int \mathrm{d}\boldsymbol{r} n_{0i} \ln g_{ii} \tag{9}$$

where g_{ii} is the contact value of the correlation function between segments of species i, given by

$$g_{ii} = \frac{1}{1-n_3} + \frac{3}{2}\frac{n_2\sigma_i}{(1-n_3)^2} + \frac{1}{2}\frac{{n_2}^2{\sigma_i}^2}{(1-n_3)^3}$$

The dispersion term is decomposed as the sum of a local contribution $F^{\mathrm{ex}}_{\text{disp-local}}$ and a nonlocal contribution $F^{\mathrm{ex}}_{\text{disp-nonlocal}}$. In the PC-SAFT EOS, the local contribution of the dispersion interaction is accounted for by perturbation from a chain-like reference fluid[9,17] using the segment–segment pair distribution function. The volume integrals with respect to the chain dispersion interaction are then simplified by a polynomial of the packing fraction up to order six. Mathematically,

$$\beta F_{\text{disp-local}} = -\pi \sum_{i,j=1,2} \int \mathrm{d}\boldsymbol{r}\Big\{ n_{0i}(\boldsymbol{r}) n_{0j}(\boldsymbol{r}) \times \Big[2J_1(\boldsymbol{r})\beta\varepsilon^{\mathrm{PC}}_{ij} + \overline{N} M^{-1}(\boldsymbol{r}) J_2(\boldsymbol{r}) \Big(\beta\varepsilon^{\mathrm{PC}}_{ij}\Big)^2 \Big] \sigma^3_{ij} \Big\} \quad (10)$$

where

$$M(\boldsymbol{r}) = 1 + \overline{N}\frac{8n_3 - 2{n_3}^2}{(1-n_3)^2} + (1-\overline{N})\frac{20n_3 - 27{n_3}^2 + 12{n_3}^3 - 2{n_3}^4}{(1-n_3)^2(2-n_3)^2}$$

$$J_k(\boldsymbol{r}) = \sum_{i=0}^{6} a_i^{(k)}(\overline{N})\, n_3^i,\ k = 1, 2$$

with the coefficients

$$a_i^{(k)} = a_{i0}^{(k)} + \frac{\overline{N}-1}{\overline{N}} a_{i1}^{(k)} + \frac{\overline{N}-1}{\overline{N}}\frac{\overline{N}-2}{\overline{N}} a_{i2}^{(k)},$$

In these equations, $\bar{N} = N_1 x + N_2(1-x)$ with x being the mole fraction of CO_2. The constant coefficients $\{a_{ij}^{(k)} | k = 1, 2;\ i = 0, 1, \ldots, 6; j = 0, 1, 2\}$ are given in ref. 9.

The WDA alone does not adequately describe the long-range intermolecular attractions[15] in a spatially inhomogeneous system. The additional long-range dispersion contributions due to spatial inhomogeneity are included in a mean-field manner by[16]

$$F^{\mathrm{ex}}_{\text{disp-nonlocal}}[\rho_1(\boldsymbol{r}), \rho_2(\boldsymbol{r})] = \frac{1}{4}\sum_{i,j=1,2} \iint \mathrm{d}\boldsymbol{r}\mathrm{d}\boldsymbol{r}' \Theta\big(|\boldsymbol{r}-\boldsymbol{r}'| - \sigma_{ij}\big) u_{ij}(|\boldsymbol{r}-\boldsymbol{r}'|) \times \big[\rho_i(\boldsymbol{r}) - \rho_i(\boldsymbol{r}')\big]\big[\rho_j(\boldsymbol{r}) - \rho_j(\boldsymbol{r}')\big] \quad (11)$$

This form ensures that $F^{\mathrm{ex}}_{\text{disp-nonlocal}}$ vanishes for the uniform bulk state and hence does not overcount the contribution already included in the bulk EOS. The step function $\Theta(\boldsymbol{r} - \sigma_{ij})$ can be considered the zero-density value of the pair distribution function $g_{ij}(|\boldsymbol{r} - \boldsymbol{r}'|)$. Because of the long-range nature of the dispersion interaction, we expect that this approximation that essentially amounts to averaging out oscillations in the g_{ij} should be a reasonable one. Note that the form of eqn (11) is not to be confused with a commonly adopted mean-field treatment of dispersion interactions in the form

$$F^{\mathrm{ex}}_{\text{disp}}[\rho_1(\boldsymbol{r}), \rho_2(\boldsymbol{r})] = \frac{1}{2}\sum_{i,j=1,2} \iint \mathrm{d}\boldsymbol{r}\mathrm{d}\boldsymbol{r}' \Theta\big(|\boldsymbol{r}-\boldsymbol{r}'| - \sigma_{ij}\big) \times u_{ij}(|\boldsymbol{r}-\boldsymbol{r}'|)\rho_i(\boldsymbol{r})\rho_j(\boldsymbol{r}')$$

which is known to be inaccurate for describing equilibrium bulk phase behavior and interfacial properties.[18–20] The use of the segment–segment pair distribution function based on a chain-like reference state in eqn (10) includes essential correlation effects from both packing and chain connectivity neglected in a mean-field approach. Our mean-field approximation only concerns the *additional* long-range nonlocal term $F_{\text{disp-nonlocal}}$, eqn (11), which does not affect the thermodynamics in a uniform bulk system. The combined eqn (10) and (11) provide accurate description for both the bulk thermodynamic behavior and interfacial properties, as demonstrated in our recent work.[8]

The grand potential W of the system is related to the Helmholtz free energy functional as

$$W = F - \mu_1 \int \rho_1(\boldsymbol{r})\mathrm{d}\boldsymbol{r} - \mu_2 \int \hat{\rho}_2(\boldsymbol{r}^{N_2})\mathrm{d}\boldsymbol{r}^{N_2} \quad (12)$$

where μ_1 and μ_2 are the chemical potential of CO_2 and the polymer chain, respectively.

4. String method

Inasmuch as bubble nucleation can be considered an activated rare event, we adopt a thermodynamic approach in which nucleation is treated as a localized fluctuation in an open system with a fixed chemical potential for each species set by the metastable bulk phase. We consider the nucleation of a single spherical CO_2 bubble from the bulk polymer–CO_2 mixture, with the origin of the coordinate system taken to be at the center of the bubble. Because of spherical symmetry, the density profiles are only functions of the radial coordinate r.

The key properties of interest are the free energy barrier—the free energy at the transition state—and the nucleation path. In a mean-field framework, nucleation proceeds along the minimum free energy path (MFEP) on the functional space of grand potential $W[\rho_1(r), \rho_2(r)]$, where ρ_1 and ρ_2 are the number density of CO_2 and polymer segments, respectively. The MFEP $\{\rho_j(r, s) | j = 1, 2;\ 0 \le s \le 1\}$ (where s is the normalized reaction coordinate on the path) connects the initial state $\{\rho_j(r, 0)\}$ (the metastable bulk state of mixtures) and the final state $\{\rho_j(r, 1)\}$ (a well-developed bubble) *via* a path that passes through the transition state (saddle point on the free energy surface). It is defined such that the tangent along the path is parallel to the free energy gradient,

$$\begin{cases} \dfrac{\delta W}{\delta\rho_1} - \left(\tau_1 * \dfrac{\delta W}{\delta\rho_1}\right)\tau_1 = 0 \\ \dfrac{\delta W}{\delta\rho_2} - \left(\tau_2 * \dfrac{\delta W}{\delta\rho_2}\right)\tau_2 = 0 \end{cases} \quad (13)$$

where

$$\tau_j(r,s) = \frac{\partial \rho_j(r,s)}{\partial s} \Big/ \left(\frac{\partial \rho_j(r,s)}{\partial s} * \frac{\partial \rho_j(r,s)}{\partial s} \right)^{1/2}$$

is the normalized tangent along the path and * denotes the inner product defined as $f * g = \int f(r)g(r)\mathrm{d}r$. Eqn (13) is then solved by using the string method,[10] which is a modified steepest descent algorithm,

$$\begin{cases} \dfrac{\partial \rho_1(r,s;t)}{\partial t} = -\left[\dfrac{\delta W}{\delta \rho_1} - \left(\tau_1 * \dfrac{\delta W}{\delta \rho_1} \right) \tau_1 \right] + k_1 \tau_1 \\ \dfrac{\partial \rho_2(r,s;t)}{\partial t} = -\left[\dfrac{\delta W}{\delta \rho_2} - \left(\tau_2 * \dfrac{\delta W}{\delta \rho_2} \right) \tau_2 \right] + k_2 \tau_2 \end{cases} \quad (14)$$

where k_1 and k_2 are Lagrange multipliers introduced to enforce the particular parameterization of the string one chooses (for example by normalizing its arc length),[21] and t is a fictitious time for evolving the equations on the free energy landscape. We adopt an explicit forward time splitting to solve eqn (14). The iteration starts with a set of initial density profiles ($t = 0$) between the initial state ($s = 0$, the uniform metastable bulk) and the terminal state ($s = 1$, a well developed bubble, see below). States between $s = 0$ and $s = 1$ are obtained by linear interpolation. After each iteration, we reparameterize the states of density profile equidistantly along the path. The process ends when the maximum difference between the free energy along the path between two consecutive iterations is less than 10^{-5}.

The density profiles of the terminal state are determined by a constrained method proposed in ref. 22. In this method, a particular value of the density of one of the component, say the polymer, is assigned to a particular radial distance R. The value of the density is intermediate between those for the two coexisting phases; a convenient choice is $\rho_2(R) = (\rho_2^{\mathrm{center}} + \rho_2^{\mathrm{bulk}})/2$, where ρ_2^{bulk} is the density in the metastable bulk phase and ρ_2^{center} is the polymer density at the center of a well-developed nucleus determined by equality of chemical potential with the bulk metastable phase

$$\mu_j(\rho_1^{\mathrm{center}}, \rho_2^{\mathrm{center}}) = \mu_j(\rho_1^{\mathrm{bulk}}, \rho_2^{\mathrm{bulk}}), j = 1, 2 \quad (15)$$

The constraint essentially corresponds to fixing the location of the interface. With this constraint serving as a boundary condition, we then minimize the grand potential functional by setting

$$\frac{\delta W}{\delta \rho_1(r)} = 0, \quad \frac{\delta W}{\delta \rho_2(r)} = 0 \quad (16)$$

Note that the second part of the variation condition only applies for $r \neq R$ because of the boundary condition. We choose R to be sufficiently large that the density profiles of the well-developed bubble become insensitive to the value of R. In most cases, we find $R = 10$ nm to be sufficient.

5. Results and discussion

5.1. Metastable condensation phase transition

Nucleation is initiated by a pressure drop from a high initial pressure P_0 at the coexistence (*i.e.* a CO_2 saturated polymer liquid) to the ambient pressure 0.1 MPa, see Fig. 1. The density is allowed to relax, while maintaining the same composition (weight fraction of CO_2, w) at the new pressure value, resulting in a metastable bulk state highly supersaturated with CO_2. The initial pressure P_0 thus controls the composition of the metastable state and its degree of supersaturation.

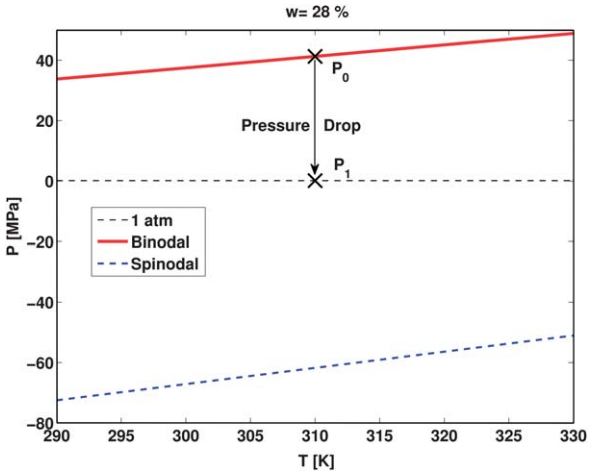

Fig. 1 Phase diagram of PMMA–CO_2 mixtures at $w = 28\%$ weight fraction of CO_2. Nucleation is initiated by a pressure drop from the coexistence (initial pressure, P_0) to the pressure (nucleation pressure, P_1) where nucleation takes place.

We note that both pure PMMA and pure PS are glassy in the temperature ranges we consider in our calculation. However, dissolution of compressed CO_2 can considerably suppress the glass transition temperature T_g of the polymer.[23–25] For PMMA, T_g is suppressed to about 280 K,[26] when saturated with CO_2 in the pressure range of 5–25 MPa, which is below the temperature range we consider here. For PS, with a saturation pressure of CO_2 in the range of 10–30 MPa, T_g occurs around 305 K.[26] However, nucleation takes place at an ambient pressure of 0.1 MPa in a CO_2-supersaturated metastable state. Because there is more free volume at the lower pressure, while the CO_2 content remains high, it is likely that T_g for the metastable PS–CO_2 mixture can be well below 305 K. In this work, we will assume that the polymer mixture is in the liquid state. Nevertheless, we recommend caution in interpreting our PS–CO_2 results for temperatures below 305 K.

In the region near the critical temperature of CO_2, a CO_2-rich liquid (CRL) and a CO_2-rich vapor (CRV) can coexist with the polymer-rich phase, giving rise to an equilibrium triple line. The effects of this equilibrium triple line on nucleation in generic binary mixtures and in model polymer–CO_2 mixtures have been previously elucidated.[6] However, in the CO_2 supersaturated metastable polymer-rich phase at ambient pressure, at the same respective chemical potential for CO_2 and polymer, there can also exist metastable CRV and CRL phases whose densities are determined by eqn (15). These metastable phases are lower in their grand potential density than the parent metastable phase (which is just the negative of the ambient pressure, *i.e.* −0.1 MPa). Since the initial stage of nucleation occurs at constant chemical potential, it is these metastable phases, rather than the equilibrium CRV at the ambient pressure, that form the

nuclei of the initial bubble nucleation. The metastable CRV–CRL transition and its consequence on bubble nucleation in the PMMA–CO_2 system have been reported in a recent communication.[11] Here we focus on the case of PS–CO_2. Fig. 2(a) shows the grand potential density (*i.e.*, negative of the pressure) of these two metastable phases for PS–CO_2 mixtures as a function of the initial pressure P_0. At $T = 300$ K, the CRV crosses the CRL phase at $P_0 = 33.6$ MPa, corresponding to a metastable condensation transition. The CRV phase persists until $P_0 \leq 39.2$ MPa and the CRL phase starts to appear at $P_0 \geq 28.5$ MPa. These pressures define the respective spinodals for the CRV and CRL phases. Between these spinodals, both CRV and CRL phases can exist. As temperature increases, the spinodal pressure of the CRV decreases while that of the CRL increases, until they converge to a critical point at $T_c = 306.8$ K. For $T > T_c$, the CO_2-rich metastable phase becomes supercritical. Fig. 2(b) shows the metastable spinodal lines as well as the condensation transition line in the P_0–T plane. We emphasize that this metastable "phase diagram" is only meaningful in the context of the metastable PS-rich parent phase; the metastable CRV and CRL do not exist on their own as a bulk state.

The "phase diagram" shown in Fig. 2(b) provides a global map for the nucleation behavior. For $T \geq T_c$, the mixture nucleates to a supercritical CO_2-rich bubble. For $T < T_c$, below the metastable spinodal pressure of the CRL, CRL does not exist, and so nucleation can only be to the CRV state. In the region above the metastable spinodal of the CRV, the mixture can only nucleate a CRL bubble. In the region between these two spinodals, both CRL and CRV phases can exist as metastable states having lower free energy than the parent metastable phase. The nucleating bubble can therefore correspond to either the CRV or the CRL phase; the actual nucleation path is the one of the lowest free energy barrier.

Compared with the case of PMMA–CO_2, the metastable spinodal curve of CRV in the case of PS–CO_2 has a stronger curvature. The locations of the condensation line and the critical point are similar in both systems. However, we will show that the free energy barrier for bubble nucleation in PS–CO_2 is much higher than in PMMA–CO_2 under the same nucleation conditions.

5.2. Nucleation below T_c

We first consider nucleation at $T < T_c$. We have calculated the nucleation properties to both CRV and CRL. The results are shown in Fig. 3(a) and (b). Clearly, for all P_0, nucleation to the CRL phase has a lower barrier. While this behavior is consistent with the Ostwald's step rule[27] before the condensation point—since the free energy of the CRL is closer to the metastable parent phase than CRV, this rule does not apply after the condensation point. Exceptions to Ostwald's rule have also been reported in the crystallization of minerals.[28,29]

As shown in Fig. 3(a), below the metastable critical point, the nucleation barrier to the CRL branch is always lower than to the CRV branch, and so the preferred nucleation path is the one to the CRL branch. This suggests the following scenario for the nucleation behavior in the mixture. For initial pressure P_0 below the spinodal value of the CRL phase, only a CRV nucleus is

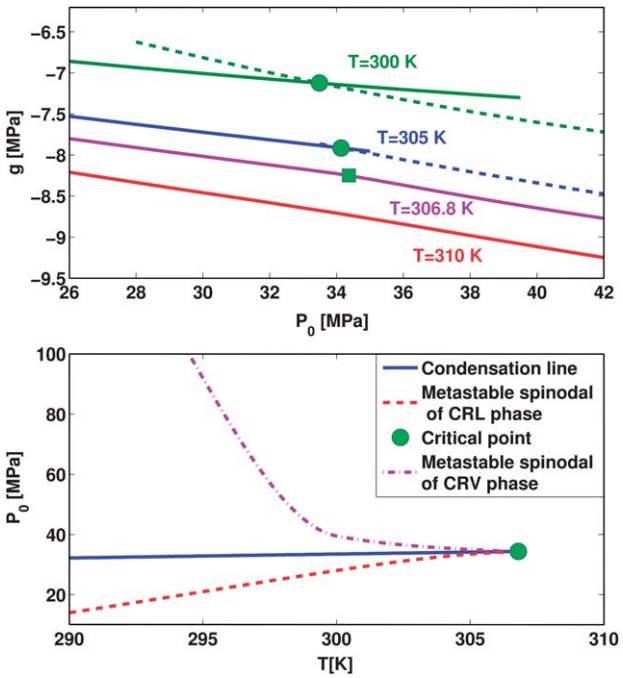

Fig. 2 (a) Grand potential density of the metastable CO_2-rich phases determined from the equal chemical potential condition with the metastable parent PS-rich liquid at ambient pressure 0.1 MPa for $T = 300$ K (dark green lines), 305 K (blue lines), 306.8 K(purple lines) and 310 K(red lines). The solid lines at $T = 300$ K and 305 K are CRV phases and the dashed lines are CRL phases, respectively. The solid circles denote the metastable condensation points, and the solid square is the metastable critical point. (b) Phase diagram for the metastable CO_2-rich phases in $T - P_0$ plane at the nucleation pressure of 0.1 MPa.

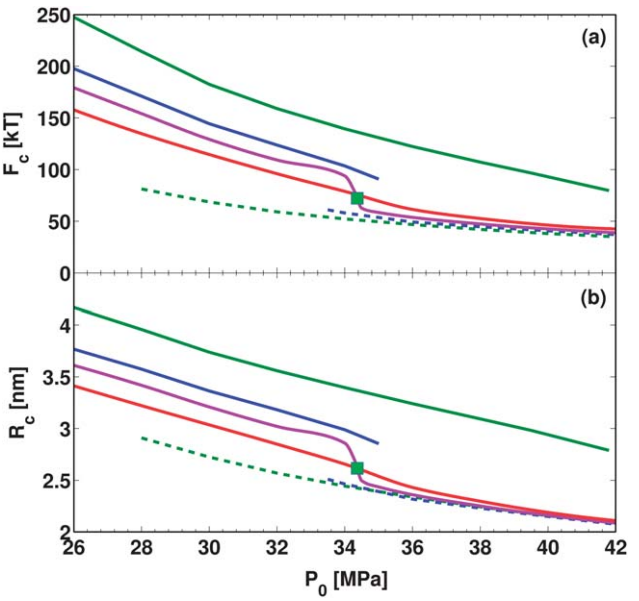

Fig. 3 (a) and (b) Free energy barrier and radius of the critical nucleus for the PS–CO_2 system as a function of the initial pressure for $T = 300$ K (dark green lines), 305 K (blue lines), 306.8 K (purple lines) and 310 K (red lines). The solid lines at $T = 300$ K and 305 K are CRV phases and the dashed lines are CRL phases, respectively.

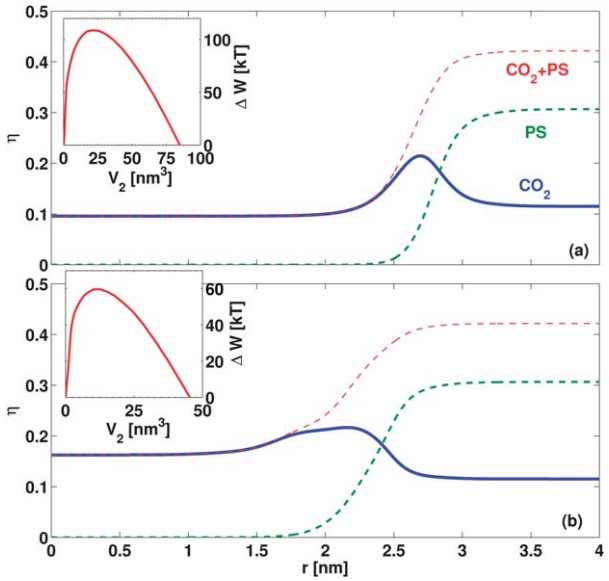

Fig. 4 (a) and (b) Dimensionless density profiles of the two types of critical nucleus for $P_0 = 33.4$ MPa (CRV nucleus) and $P_0 = 33.5$ MPa (CRL nucleus), respectively, at $T = 305$ K. The insets show the excess free energy ($\Delta W = W - W_{bulk}$) of bubble formation as a function of PS deficiency in the bubble $\left(V_2 = -4\pi\int_0^\infty dr r^2\left[\rho_2(r) - \rho_2^{bulk}\right]\right)$.

possible, which, however, requires a rather high nucleation barrier, making bubble nucleation an unlikely event. Upon increasing P_0 to the spinodal of the CRL, there is a precipitous drop in the nucleation barrier, as the nucleating phase now becomes CRL. In other words, we expect a sudden increase in the nucleation rate as a function of the initial pressure P_0. Fig. 4 shows the dimensionless density profiles (packing fractions) of the critical nucleus and the free energy barrier across the discontinuous jump (*i.e.* the metastable spinodal of CRL) at $T =$ 305 K. The packing fraction is defined as $\eta_i = (\pi/6)\rho_i\sigma_i^3$, where σ_i is the diameter of CO_2 molecules ($i = 1$) or polymer segments ($i = 2$). Obviously, the CRL nucleus (Fig. 4(b)) has a higher CO_2 density in the interior than in the CRV nucleus (Fig. 4(a)). For the CRV nucleus (Fig. 4(a)), the CO_2 density is significantly enhanced at the interface. Interestingly, the density of CO_2 inside the nucleus is less than in the parent phase. For the CRL nucleus, the width of the interfacial region is wider and the enhancement of the CO_2 density is less. We note that the location of this discontinuity for the PMMA–CO_2 system is within the range of experimental pressures for polymer foaming.[30] Therefore, the phenomenon predicted here should be readily observable.

Because the equilibrium coexisting CO_2-rich phase at the nucleation pressure (*i.e.* 0.1 MPa) is a vapor, the CRL nucleus will eventually turn into CRV. This process may take the form of another nucleation of the CRV from a well-developed CRL bubble, which, however, will require another barrier. The more likely scenario is that as the CRL bubble grows, depletion of CO_2 from the polymer-rich parent phase becomes significant, and with the decrease in the chemical potential of CO_2, the CRL bubble evaporates to become CRV, with no barrier or a much reduced barrier. Since the process involves the growth of the post-critical nucleus bubble and a changing chemical potential, it can no longer be treated within the existing thermodynamic framework in which nucleation takes place at constant reservoir conditions supplied by the bulk metastable parent phase. Regardless of how the CRV appears in the CRL bubble, bubble formation at initial pressures exceeding the spinodal value of the CRL will be a two-step process, first the formation of a CRL nucleus and then the transformation of CRL into a CRV. Two-step nucleation processes have also been suggested for a number of other systems.[31]

The nucleation barrier for PS–CO_2 shown in Fig. 3 is significantly higher than that for PMMA–CO_2.[11] A simple explanation is that, at the same T and P_0, the CO_2 solubility in the PS liquid is lower than in the PMMA liquid.[8] Moreover, at the same weight fraction of CO_2, the spinodal value of PS–CO_2 is also lower than that of PMMA–CO_2, which leads to a lower degree of supersaturation for the metastable fluid at the ambient pressure. As the pressure is the controlling variable, we define a relative degree of supersaturation S using the difference between the binodal pressure P_b and the nucleation pressure P_1, scaled by the difference between the binodal pressure and the spinodal pressure P_s for a given weight fraction of CO_2, *i.e.* $S \equiv (P_b - P_1)/(P_b - P_s)$. In this definition, the nucleation barrier is infinite at $S = 0$ and vanishes at $S = 1$. Fig. 5 compares S for nucleation at the ambient pressure ($P_1 =$ 0.1 MPa) for PS–CO_2 and for PMMA–CO_2 as a function of temperature at $w = 25\%$. We see that to get the same value of S, the temperature of the PS–CO_2 system has to be higher than that of the PMMA–CO_2. For example, at $S = 0.25$, the temperature of PMMA–CO_2 is 302.6 K, while it is 317.0 K for PS–CO_2. Moreover, to have the same CO_2 solubility in PS as in PMMA, a higher initial pressure P_0 is also required. To reach $w = 25\%$, $P_0 = 24.01$ MPa for PMMA at $T = 302.6$ K but $P_0 =$ 30.62 MPa is required for PS at $T = 317$ K. Therefore, to get the same nucleation barrier at the ambient pressure, both the nucleation temperature and the initial pressure have to be higher for PS–CO_2 than that for PMMA–CO_2.

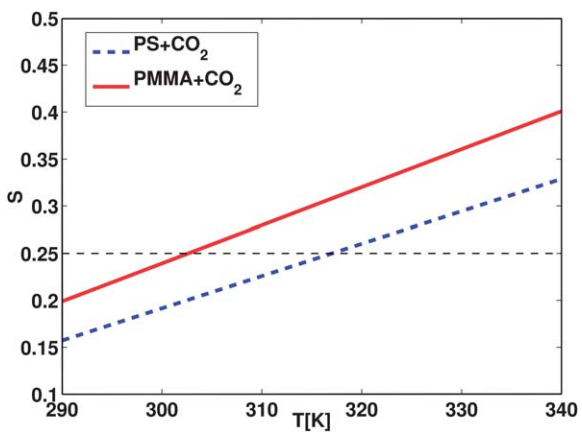

Fig. 5 Effect of temperature on the relative degree of supersaturation ($S = (P_b - 0.1)/(P_b - P_s)$) in the metastable bulk phase at a CO_2 weight fraction of $w = 25\%$.

5.3. Nucleation above T_c

We now consider nucleation in the supercritical state, $T > T_c$. While going through the CRL branch leads to a faster nucleation in the formation of the bubbles, the resulting gas bubbles can be quite large since the CRV is formed at a later stage. In order to produce small bubbles with high density, it is better to induce nucleation in the supercritical states, where the nucleation barrier decreases smoothly with increasing initial pressure and the critical nucleus sizes are relatively small. As our communication has only shown the nucleus structure for PMMA–CO_2 at temperatures less than T_c, here for completeness we show in Fig. 6 the evolution of the density profiles for a bubble along the MFEP at $T = 310$ K ($>T_c$) for the same PMMA–CO_2 mixture. The set of images from (a) to (i) show the evolution of the density profiles for PMMA (green lines), CO_2 (blue lines) and the total density (red lines) of both species. Clearly, the classical nucleation theory (CNT) cannot describe any of the structural features. Some of the structural features also cannot be captured using crude theories based on incompressible, pseudo-one-component treatment of the polymer–CO_2 mixture.[32] At the very early stage of bubble formation (Fig. 6(b)), the total density profiles exhibit a slight oscillation. The CO_2 density overshoots (*i.e.*, exceeds the bulk coexistence value and the value in the well-developed bubble) on its way to the critical nucleus. When the bubble becomes large enough, the density in the core decreases to a value of slightly higher than the bulk density of CO_2. We also see a notable enhancement of CO_2 at the bubble interface.

Of central importance is the excess free energy ($\Delta W = W - W_{bulk}$, where W_{bulk} is the grand potential in bulk phase) of bubble formation as a function of the PMMA deficiency in the bubble (defined as $V_2 = -4\pi \int_0^\infty \left[\rho_2(r) - \rho_2^{bulk}\right] r^2 dr$) along the nucleation path (the MFEP); this is shown in Fig. 7(a). The free energy barrier is 23.26 kT, which corresponds to moderately fast nucleation kinetics. For comparison, in the same figure we include results from the CNT. In the CNT, the free energy to form a bubble of radius R consists of a surface term and a volume term,

$$\Delta W_{CNT} = 4\pi R^2 \gamma + \frac{4\pi R^3}{3}(g_{center} - g_{bulk}) \quad (17)$$

where γ is usually taken as the equilibrium interfacial tension, and g_{center} and g_{bulk} are the grand potential density at the center of a well-developed nucleus and in the metastable bulk phase, respectively. The result from the CNT using the equilibrium interfacial tension ($\gamma = 2.20$ mN m^{-1}) is given by the blue dashed curve. Clearly, the CNT drastically underestimates the free energy. We have also constructed a modified CNT with a fitted value of interfacial tension ($\gamma = 5.61$ mN m^{-1}) by using the asymptotic behavior of the free energy at large V_2, in part to account for the nonequilibrium nature of the interface. The modified CNT is closer to the result obtained from the string method, but the discrepancy is still quite large. For very large bubbles, because of the dominance of the volume term, all three curves show the same limiting slope on the log–log plot, see

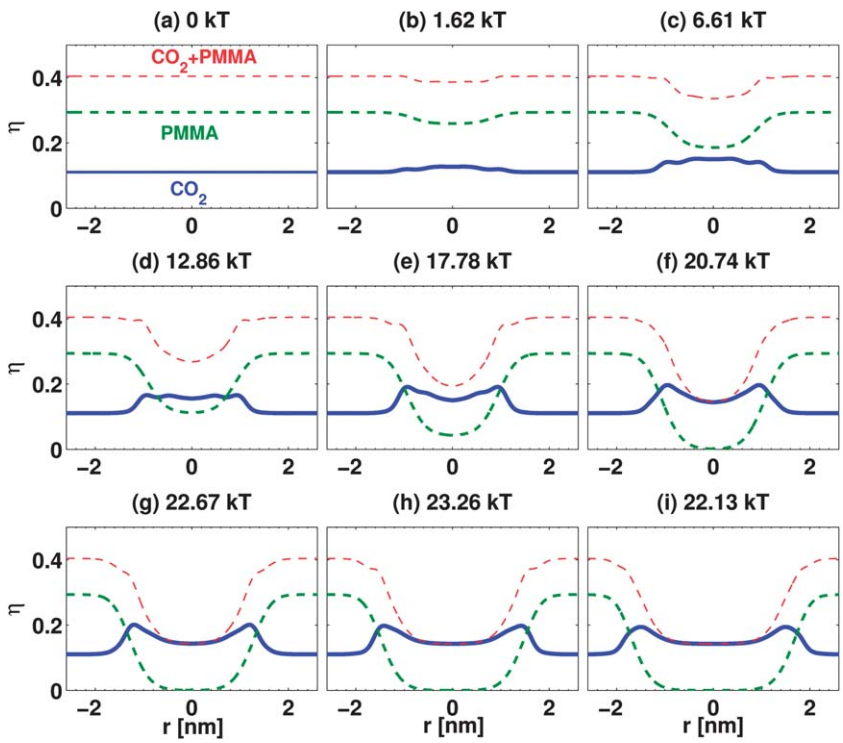

Fig. 6 Evolution of the dimensionless density profiles for a CO_2 bubble along the minimum free energy path (MFEP) in the PMMA–CO_2 mixture in the supercritical state. Nucleation is initiated by a pressure drop from the coexistence point $P_0 = 41.3$ MPa to $P_1 = 0.1$ MPa at $T = 310$ K. (h) Corresponds to the critical nucleus. The excess free energy is shown above each panel.

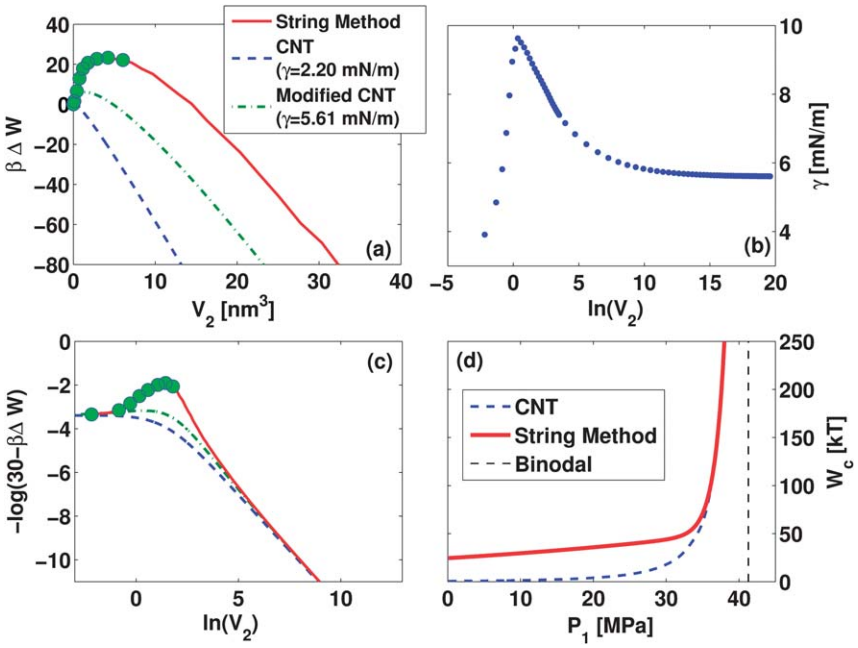

Fig. 7 Comparison between the string method and the CNT. (a) Formation free energy of the bubble nucleus as a function of PMMA deficiency V_2. Nucleation is initiated by a pressure drop from the coexistence point $P_0 = 41.3$ MPa to $P_1 = 0.1$ MPa at $T = 310$ K. The solid circles correspond to states shown in Fig. 6. (b) Effective interfacial tension implied by the CNT as a function of $\log(V_2)$. (c) log–log plot of (a). (d) Free energy barrier as a function of nucleation pressure (P_1). The initial coexisting pressure is $P_0 = 41.3$ MPa. In taking the logarithm of the PMMA deficiency V_2, a reference volume of 1 nm^3 is used.

Fig. 7(c). The modified CNT converges to the result calculated by the string method; CNT does not converge to the same limiting values, as the value of the interfacial tension is different. However, in order to have large *critical* nuclei, the system must be close to the binodal, but in that case the nucleation barrier is too high to be relevant. Fig. 7(d) shows the nucleation barrier as a function of the nucleation pressure (P_1). One can see that the results from the CNT and from the string method agree well as the nucleation pressure approaches the binodal pressure ($P_0 =$ 41.3 MPa). However, for nucleation at the ambient pressure $P_1 = 0.1$ MPa, the nucleation barrier predicted by the CNT is far too low. That the CNT underestimates the free energy barrier for nucleation in single component fluids has also been pointed out by previous theoretical studies.[33–35] To understand this behavior, we note that at the early stage of bubble formation, change in the density profile from the metastable parent phase is quite small (see the density profiles in Fig. 6(a)–(f)), resulting in a small difference in the grand potential density difference in the volume contribution. In CNT, on the other hand, this difference is fixed at $g_{\text{center}} - g_{\text{bulk}}$. As this difference is negative, overemphasis of this term in the CNT leads to an underestimate of the free energy if one uses a constant equilibrium interfacial tension or a fitted value from subtracting the volume term at large radius. Indeed, if one insists on a constant $g_{\text{center}} - g_{\text{bulk}}$, as in the CNT, then the difference between the total excess free energy and the volume term alone can be used to define an effective interfacial tension. This tension is clearly a function of the nucleus size and only reaches the asymptotic value of $\gamma =$ 5.61 mN m^{-1} when the bubble is sufficiently large. For bubble sizes near the critical nucleus, the effective tension is considerably higher than both the equilibrium value and the fitted asymptotic value. Therefore, using either these tension values together with the constant $g_{\text{center}} - g_{\text{bulk}}$ will always yield an underestimate of the free energy.

6. Conclusions

In conclusion, using our recently developed DFT, we have studied bubble nucleation in both PMMA–CO_2 and PS–CO_2 mixtures. Nucleation is induced by saturating the polymer fluid with high pressure CO_2 and subsequently decreasing the pressure to ambient condition. The minimum free energy path on the free energy landscape—the mean-field nucleation pathway—is calculated by the string method. Our calculation shows that below a metastable condensation critical temperature, there are two possible states for the CO_2-rich nucleus: a CO_2-rich vapor (CRV) like state or a CO_2-rich liquid like state, depending on the initial pressure, with the CRL nucleus generally having a lower free energy barrier. The existence of these two metastable states for the nucleus is bracketed by their respective spinodal. Because the actual nucleation pathway is the one with the lowest barrier, this result implies that as the initial pressure increases past the spinodal for the CRL, the nucleated state should jump discontinuously from the CRV branch to the CRL branch with a precipitous reduction in the free energy barrier and the radius of critical nucleus. The location of this discontinuity is within the experimental range of pressures used for foaming. As a result of the intervention of the CRL, the formation of CO_2-rich gas bubbles will be a two-step process: the formation of the CRL nucleus and further

nucleation or growth into the CO_2-rich gas. At the supercritical temperatures, the nucleation barrier decreases smoothly with increasing initial pressure and the critical nucleus sizes are relatively small. These results suggest that for the purpose of producing nanocell polymer foams with maximal cell nucleation density, the nucleation temperature should preferably be above the critical temperature of the metastable condensation.

Our study also shows that at the same temperature and pressure conditions, the barrier for bubble nucleation is higher in the PS–CO_2 mixture than in the PMMA–CO_2. For example, at $T = 310$ K and $P_0 = 35$ MPa, the nucleation barrier is 69.42 kT for PS–CO_2, while it is 37.06 kT for PMMA–CO_2 mixtures. However, this result is not only a consequence of the lower solubility of CO_2 in PS than in PMMA. Even at the same solubility (which will require a higher initial pressure for the PS–CO_2 system), the nucleation temperature for PS–CO_2 has to be about 15 K higher than for PMMA–CO_2 to reach a similar driving force for nucleation. These results may offer a possible explanation for the fact that foaming is more difficult in PS–CO_2 than in PMMA–CO_2 and suggest that both the temperature and the initial pressure need to be higher for PS–CO_2 than for PMMA–CO_2 in order to increase the foamability in the PS–CO_2 mixture.

Within the framework of mean field theory, the present work represents the most advanced and accurate methodology in treating nucleation of polymer–CO_2 mixtures. The quantitative accuracy of our DFT enables specific numerical predictions that can be directly tested by experiments. The key features reported in this work are incapable of being captured by either the classical nucleation theory or previous self-consistent field theory based on an incompressible, pseudo-single-component model for the mixture.[32] The combination of the string method and accurate DFT opens the way for studying nucleation in complex polymeric systems, such as polymer–CO_2 mixtures in the presence of nanoparticles[36] and polymer–polymer–CO_2 mixtures.[37]

Acknowledgements

The Dow Chemical Company is acknowledged for funding and for permission to publish the results. The computing facility on which the calculations were performed is supported by an NSF-MRI grant, Award no. CHE-1040558.

References

1 A. Nawaby, Y. Handa, X. Liao, Y. Yoshitaka and M. Tomohiro, *Polym. Int.*, 2007, **56**, 67–73.
2 K. Binder, B. M. Mognetti, L. G. Macdowell, M. Oettel, W. Paul, P. Virnau and L. Yelash, *Macromol. Symp.*, 2009, **278**, 1–9.
3 K. Binder, M. Müller, P. Virnau and L. G. MacDowell, *Adv. Polym. Sci.*, 2005, **173**, 1–104.
4 P. Virnau, M. Müller, L. G. MacDowell and K. Binder, *New J. Phys.*, 2004, **6**, 7.
5 X. C. Zeng and D. W. Oxtoby, *J. Chem. Phys.*, 1991, **95**, 5940–5947.
6 M. Müller, L. G. MacDowell, P. Virnau and K. Binder, *J. Chem. Phys.*, 2002, **117**, 5480–5496.
7 A. Laaksonen, V. Talanquer and D. W. Oxtoby, *Annu. Rev. Phys. Chem.*, 1995, **46**, 489–524.
8 X. F. Xu, D. E. Cristancho, S. Costeux and Z.-G. Wang, *J. Chem. Phys.*, 2012, **137**, 054902.
9 J. Gross and G. Sadowski, *Ind. Eng. Chem. Res.*, 2001, **40**, 1244–1260.
10 E. Weinan and E. Vanden-Einden, *Annu. Rev. Phys. Chem.*, 2010, **61**, 391–420.
11 X. F. Xu, D. E. Cristancho, S. Costeux and Z.-G. Wang, *J. Phys. Chem. Lett.*, 2013, **4**, 1639–1643.
12 Y. Rosenfeld, *Phys. Rev. Lett.*, 1989, **63**, 980–983.
13 Y. X. Yu and J. Z. Wu, *J. Chem. Phys.*, 2002, **117**, 10156–10164.
14 E. Kierlik and M. L. Rosinberg, *J. Chem. Phys.*, 1993, **99**, 3950–3965.
15 P. Tarazona, J. Cuesta and Y. Martinez-Raton, *Lect. Notes Phys.*, 2008, **753**, 247–341.
16 C. Ebner, W. F. Saam and D. Stroud, *Phys. Rev. A*, 1976, **14**, 2264–2273.
17 J. Gross and G. Sadowski, *Fluid Phase Equilib.*, 2000, **168**, 183–199.
18 H. Kahl and J. Winkelmann, *Fluid Phase Equilib.*, 2008, **270**, 50–61.
19 Z. Tang, L. E. Scriven and H. T. Davis, *J. Chem. Phys.*, 1991, **95**, 2659–2668.
20 X. Xu, D. Cao and J. Wu, *Soft Matter*, 2010, **6**, 4631–4646.
21 W. N. E. W. Ren and E. Vanden-Eijnden, *J. Chem. Phys.*, 2007, **126**, 164103.
22 S. M. Wood and Z.-G. Wang, *J. Chem. Phys.*, 2002, **116**, 2289–2300.
23 W. C. V. Wang, E. J. Kramer and W. H. Sachse, *J. Polym. Sci., Part B: Polym. Phys.*, 1982, **20**, 1371–1384.
24 R. G. Wissinger and M. E. Paulaitis, *J. Polym. Sci., Part B: Polym. Phys.*, 1991, **29**, 631–633.
25 P. D. Condo, I. C. Sanchez, C. G. Panayiotou and K. P. Johnston, *Macromolecules*, 1992, **25**, 6119–6127.
26 C. Dutriez, K. Satoh, M. Kamigaito and H. Yokoyama, *RSC Adv.*, 2012, **2**, 2821–2897.
27 W. Ostwald, *Z. Phys. Chem.*, 1897, **22**, 289–330.
28 J. C. Deelman, *Chemie der Erde*, 2001, **61**, 224–235.
29 L. O. Hedges and S. Whitelam, *J. Chem. Phys.*, 2011, **135**, 164902.
30 J. A. Reglero Ruiz, M. Pedros and M. Dumon, *J. Supercrit. Fluids*, 2011, **58**, 168–176.
31 P. G. Vekilov, *J. Cryst. Growth*, 2005, **275**, 65–76.
32 Y. Kim, C. B. Park, P. Chen and R. B. Thompson, *Soft Matter*, 2011, **7**, 7351–7358.
33 M. Iwamatsu, *J. Chem. Phys.*, 2009, **130**, 244507.
34 J. F. Lutsko, *Phys. Rev. E: Stat., Nonlinear, Soft Matter Phys.*, 2006, **74**, 021603.
35 D. W. Oxtoby and R. Evans, *J. Chem. Phys.*, 1988, **89**, 7521–7530.
36 S. Costeux and L. Zhu, *Polymer*, 2013, **54**, 2785–2795.
37 S. Costeux, S. P. Bunker and H. K. Jeon, *J. Mater. Res.*, 2013, **28**, 2351–2365.